COMPOSITIONAL MAPPING OF NOACHIAN IMPACT CRATER FLOORS ON MARS. Alexander M. Sessa[1] and Sergio A. Parra[1], J. J. Wray[1], R. P. Irwin III[2], T. A. Maxwell[2], and S. C. Mest[3], [1]Georgia Institute of Technology, Atlanta, GA, [2]Smithsonian Institution, Washington, DC, [3]Planetary Science Institute, Tucson, AZ.

Introduction: On Mars, the subdued morphology and flat flooring of many Noachian impact craters can be attributed to degradation processes [1]. This progressive degradation, dependent on the age of the craters, is reflected through changes in crater geometry, with studies indicating increases in width and infilling [2, 3, 4]. These observations suggest that these impact crater floors likely hold eroded material from the walls or other surfaces beyond the craters themselves.

According to a recent survey of crater floors exhibiting this degradation, several have been noticed to have a dark cap rock above an exposed, lighter-toned stratigraphy or/in addition to wind-eroded floor materials [5, 6, 7]. Unlike basalt, which is resistant to erosion, this material is friable and susceptible to aeolian deflation, which indicates that basaltic overlays are not present in all crater floors and as such the flat flooring of Noachian impact craters may provide a valuable record of their modification.

With regards to mineral composition, near-infrared spectroscopy in recent years has revealed a prevalence of olivine and pyroxene [8] as well as phyllosilicates [9, 10], hydrated sulfates [e.g., 11], and carbonates [12] in Noachian terrains. The geographic distributions of these signatures have led to the inference of developing aqueous conditions [13, 14] and are of particular interest in the selection of landing sites for future missions [15].

Here, we describe and discuss new observations of the mineralogy of certain impact crater floors gathered from CRISM multispectral and hyperspectral imaging.

Data and Methods: We investigate the mineralogical composition of wind-eroded floor materials, as well as exposed stratigraphic layers and other corresponding geological units, contained within (and located in close proximity to) 30 Noachian impact craters in the Martian equatorial highlands (between 0–30ºS, 0–165ºE) by utilizing the Compact Reconnaissance Imaging Spectrometer for Mars (CRISM) on the Mars Reconnaissance Orbiter (MRO).

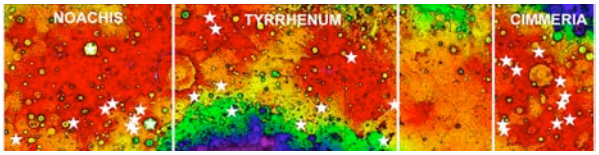

Figure 1: Study areas with 30 crater sites (stars) on MOLA base, bounded by 0ºS, 30ºS, 20ºE, and 140ºE.

These geologically diverse craters were separated into three study areas: the Terra Noachis (20–55ºE), Tyrrhena (55–100ºE), and Cimmeria (120–140ºE) regions, as shown in Figure 1.

The CRISM images obtained from the publicly released orbital datasets (available through the Planetary Data System) fall into two distinct categories: multispectral mapping mosaic tiles (MRDR) at 200 m/pixel, and hyperspectral targeted images (TRDR) at ~18 or 36 m/pixel. Each crater site also has full image coverage at ~6 m/pixel by the MRO Context Camera (CTX).

We are utilizing both CRISM observation types in order to gain a more complete geological understanding of the regions in question, with the hyperspectral images used to resolve finer-scale outcrops present within (or located in the vicinity of) specific craters in one of the three study areas. Through the additional analysis of the multispectral images, we are able to determine the relationship between units covered by multiple targeted observations within a particular area, thereby allowing a better understanding of the past geological processes that shaped this terrain.

The mineralogical assemblages of the crater-fill, visible stratigraphic layers, and other associated outcrops will be confirmed by examining the spectra from regions of interest within each CRISM image, and comparing the obtained spectra to the most recent USGS spectral library. Mapping of the mineralogical composition of the material within and around the craters has been partially accomplished by utilizing the spectral summary parameters highlighted in [16, 17].

Preliminary Observations: After stretching both multispectral and targeted hyperspectral images to obtain clear contrasts, highlighting regions of interests for a range of spectral parameters, we observed a prevalence of certain minerals within the ~15 Noachian craters analyzed so far.

In concordance with previous observations [e.g., 8], we noted very strong signatures of olivine and high-calcium pyroxene (Fig. 2). Despite the lower resolution provided by the MRDR imaging (left panels of Fig. 2), both olivine (first two rows of Fig. 2) and pyroxene (third row of Fig. 2) were identified in localized concentrations on craters floors and wall materials. These observations were further supported by co-located TRDR images (right hand panels of Fig. 2).

On the other hand, localized enhancements of other minerals were more difficult to identify in MRDR images. Parameters that, for example, track phyllosilicates, hydrated sulfates, and carbonates yielded noisy spatial distributions dominated by artifacts of scene-to-scene variations. This is consistent with the more spatially confined nature of these compositions as observed using TRDR images.

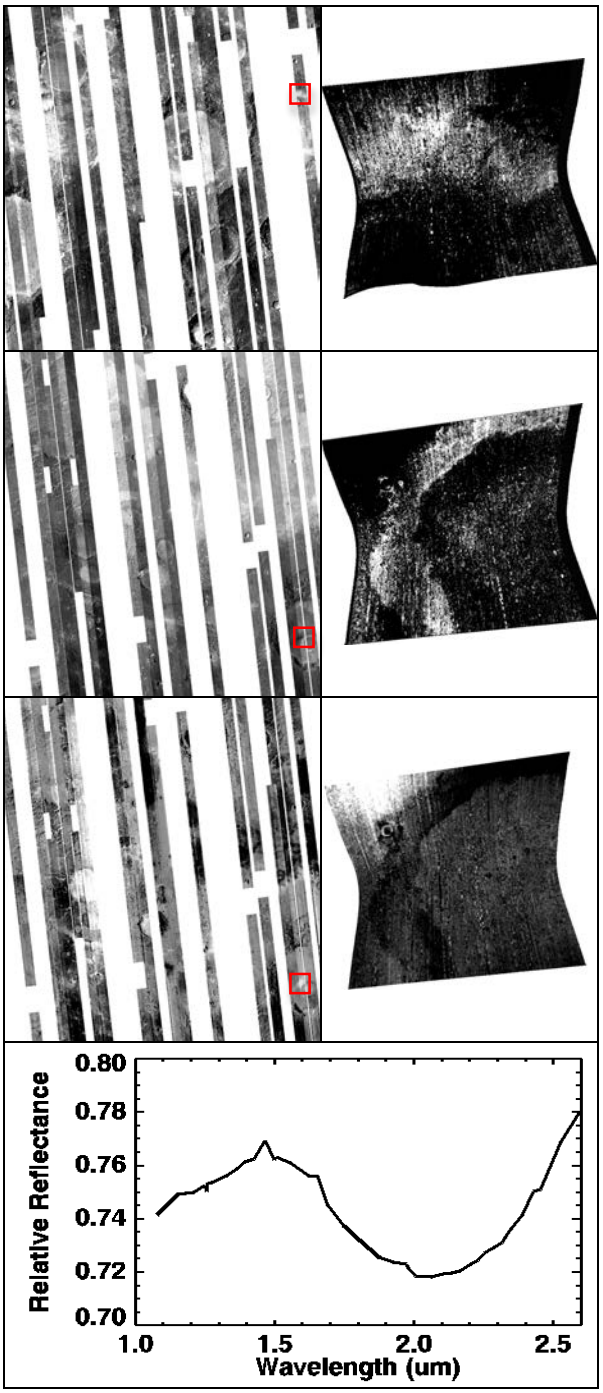

Figure 2: MRDR images are on the left, while TRDR images are on the right. From top to bottom, images are from crater 2, crater 14, and crater 14 respectively, for which we observe distinct concentrations—demarcated by red squares—of olivine (OLINDEX2), olivine (OLINDEX2), and pyroxene (HCPINDEX), as further confirmed and spatially resolved by TRDR images FRT0001171D and FRT000137E9. Bottom panel plots MRDR-derived relative reflectance as a function of wavelength (μm) from the pyroxene-enriched area in crater 14.

Figure 3 displays four TRDR observations (FRT0001171D, FRT00011ADA, HRL00013311, and FRT000136F4), which show finer-scale features such as hydrated subsurface layers exposed in the crater walls, as well as ejected subsurface material surrounding the impact basins. These hyperspectral observations are able to discern hydrated mineral-enriched materials, which make up a relatively small percentage of the pixels in these images, from the surrounding material, whereas these features were not visible in the multispectral data. In most cases, these detections show some spatial relationship (correlation or anticorrelation) with other parameters mapping the presence of olivine and pyroxene minerals, hinting at an intriguing stratigraphic history preserved at these sites.

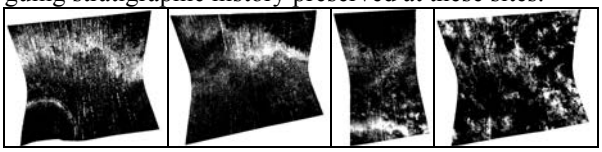

Figure 3: From left to right: Images from a subset of craters (craters 2, 4, and 6) of the CRISM summary parameter that highlights H_2O concentrations in surface material (BD3000).

Future Work: We are currently finishing the initial parameter-based mapping of mineral classes across the remaining ~15 craters highlighted in Fig. 1. Next, these identifications will be confirmed and interpreted with greater mineralogic specificity by plotting spectra (e.g., bottom of Fig. 2) and comparing them to laboratory analog spectra. Finally, we will examine visible images of each crater to determine stratigraphic relationships between the units of distinct composition, and to incorporate textural observations (e.g., styles of erosion) that will allow us to test a range of hypotheses (e.g., [18]) for the processes that have affected these crater floors throughout their history.

Acknowledgements: We thank NASA Mars Data Analysis Program grant NNX13AH80G for support.

References: [1] Craddock, R. A., and T. A. Maxwell (1993) *JGR*, *98*, 3453–3468. [2] Grant, J. A., and P. H. Schultz (1993) *JGR*, *98*, 11025−11042. [3] Craddock, R. A. et al. (1997) *JGR*, *102*, 13321–13340. [4] Forsberg-Taylor, N. K. et al. (2004) *JGR*, *109*, E05002. [5] Irwin, R. P. et al. (2010) *First Int. Conf. on Mars Sedimentology and Stratigraphy*, abstract 6028. [6] Pendrill, F. (2010) undergraduate thesis, Univ. of Gothenburg, Sweden. [7] Maxwell, T. A. et al., in prep. for *JGR*. [8] Mustard, J. F. et al. (2005) *Science, 307*, 1594–1597. [9] Poulet, F. et al. (2005) *Nature, 438,* 623–627. [10] Mustard, J. F. et al. (2008) *Nature, 454*, 305–309. [11] Wray, J. J. et al. (2009) *Geology, 37*, 1043–1046. [12] Ehlmann, B. L. et al. (2008) *Science, 322*, 1828–1832. [13] Bibring, J. P. et al. (2006) *Science*, *312*, 400–404. [14] Murchie, S. et al. (2009) *JGR, 114*, E00D06. [15] Grant, J. A. et al. (2011) *Planet. Space Sci.*, *59*, 1114–1127. [16] Pelkey, S. M. et al. (2007) *JGR*, *112*, E08S14. [17] Viviano-Beck, C. E. et al. (2014) *JGR, 119*, 1403–1431. [18] Edwards, C. S. et al. (2014) *Icarus, 228*, 149–166.